

## Phase-Matching Controlled Orbital Angular Momentum Conversion in Periodically Poled Crystals

Yan Chen,<sup>1,2,3,\*</sup> Rui Ni<sup>①,1,2,\*</sup> Yaodong Wu,<sup>1,2</sup> Li Du<sup>①,1</sup> Xiaopeng Hu<sup>①,1,2,3,†</sup> Dunzhao Wei<sup>①,1,2</sup>  
Yong Zhang<sup>①,1,2,3,‡</sup> and Shining Zhu<sup>1,2,3,§</sup>

<sup>1</sup>National Laboratory of Solid State Microstructures, College of Engineering and Applied Sciences, and School of Physics, Nanjing University, Nanjing 210093, China

<sup>2</sup>Collaborative Innovation Center of Advanced Microstructures, Nanjing 210093, China

<sup>3</sup>Key Laboratory of Intelligent Optical Sensing and Manipulation, Nanjing University, Nanjing 210093, China



(Received 8 June 2020; accepted 25 August 2020; published 29 September 2020)

Nonlinear interactions between light waves can exchange energy, linear momentum, and angular momentum. The direction of energy flow between frequency components is usually determined by the conventional phase-matching condition related to the linear momentum. However, the transfer law of orbital angular momentum (OAM) during frequency conversion remains to be elucidated. Here, we demonstrate experimentally that OAM transfer depends strongly on the phase-matching condition defined by both linear and orbital angular momenta. Under different phase-matching configurations, the second-harmonic wave exhibits variable OAM spectral characteristics such as the presence of just a single value or of odd orders only. Our results pave the way toward unveiling the underlying mechanism of nonlinear conversion of OAM states.

DOI: [10.1103/PhysRevLett.125.143901](https://doi.org/10.1103/PhysRevLett.125.143901)

The conservations of energy, linear momentum, and angular momentum are fundamental laws describing the propagation and interaction of waves in physics. In nonlinear optics, the phase-matching condition, or linear momentum conservation, allows a net positive energy flow from the fundamental wave to harmonic waves [1,2]. When light beams possessing phase singularities, i.e., vortex beams, are involved in nonlinear light-matter interactions, the transfer of orbital angular momentum (OAM) between the interacting waves must also be taken into account. A vortex beam is characterized by a spiral phase front of  $\exp(-il\theta)$ , where  $l$  is the topological charge (TC) and  $\theta$  is the azimuthal angle. Such beams carry an OAM of  $l\hbar$  per photon, and the Laguerre-Gaussian (LG) laser modes are the typical example [3]. In the past three decades, OAM has become established as an important degree of freedom in the control of light beams, and it has found a wide range of applications, including imaging, optical manipulation, high-precision optical measurement, various areas of quantum science, and optical communications [4–6]. Nonlinear generation and conversion of OAM states are of particular interest. On the one hand, through frequency conversion, vortex beams with on-demand wavelength and TC, which are not readily available using traditional methods, can be obtained [7–10]. On the other hand, links between physical systems with different operating wavelengths can be established via nonlinear frequency conversions. Examples include the creation of an entanglement link between different quantum systems operating in a photon's OAM degrees of freedom [11] and the enabling of

up-conversion detection or imaging from the infrared to the visible [12,13]. In parametric processes, the OAM is generally conserved; for example, in sum frequency generation, the OAM of the generated harmonic wave equals to the sum of the OAM carried by the input two fundamental waves (FWs) [14,15]. With regard to the OAM transfer law, in their seminal work on second harmonic generation (SHG) of LG modes, Dholakia *et al.* [16] and Courtial *et al.* [17] attributed it to be the conventional phase-matching condition; however, they considered only the linear momenta of the interacting waves. In the present work, we demonstrate experimentally that the OAM transfer in nonlinear frequency conversions depends strongly on the phase-matching condition, which is defined by both the linear and orbital angular momenta.

Here, we take typical SHG as an example, and the nonlinear material is a 1D periodically poled crystal. In periodically poled crystals, there is a periodic alternation of the ferroelectric domains of opposite spontaneous polarization. The  $n$ th-order reciprocal vector provided by the periodically poled structure can be written as  $G_n = 2\pi n/\Lambda$ , where  $\Lambda$  is the poling period. The width and length of the crystal are  $L_1$  and  $L_2$ , respectively. A general SHG of a vortex beam in the nonlinear crystal is shown schematically in Fig. 1(a), and the wave vector mismatch between the interacting waves in the  $y$  direction is

$$dk_y = -2k_{1y} - G_n \sin \theta + k_{2y'} \cos \alpha - k_{2y''} \cos \phi' \sin \alpha, \quad (1)$$

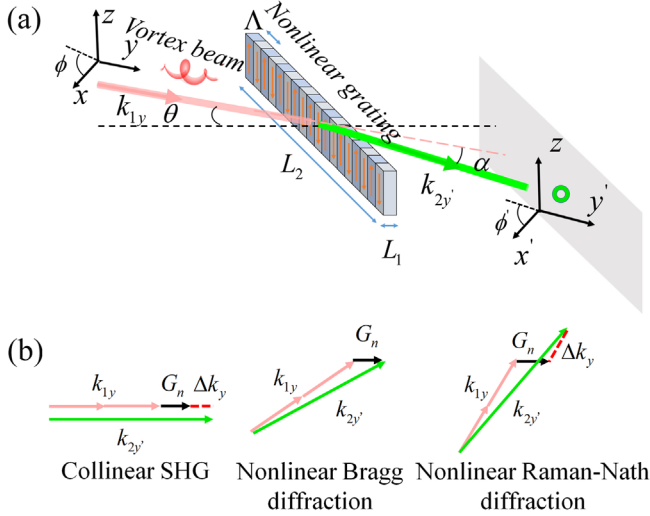


FIG. 1. (a) Schematic of a general SHG process in a periodically poled crystal (nonlinear grating). The arrows represent the directions of the spontaneous polarization. For  $\theta = 90^\circ$  and  $\alpha = 0^\circ$ , this is the collinear SHG. (b) Phase-matching configurations for collinear SHG [18], nonlinear Bragg diffraction [19], and nonlinear Raman-Nath diffraction [20].

where  $k_{2y'}$  and  $k_{2r'}$  are the wave vector components of the second harmonic (SH) wave, which are related to the linear and orbital angular momentum, respectively, and  $k_{1y}$  is the wave vector component of the FW related to the linear momentum.  $r'$  and  $\phi'$  are the radius and azimuthal angle in the  $x'$ - $z$  plane, respectively. Inside the nonlinear crystal, the angle between the FW and the domain wall is  $\theta$ , while the angle between the SH wave and the FW is  $\alpha$ .

In domain-engineered ferroelectric crystals, there are several well-established SHG phase-matching diagrams [Fig. 1(b)], which have been widely exploited for generation of new laser light sources and demonstration of novel optical effects, as well as nonlinear beam shaping [18–27]. The phase mismatches in these phase-matching diagrams are defined using the plane-wave approximation, in which only linear momenta are considered. Thus, we define two parameters to describe the phase mismatches,  $\Delta k_x \equiv -G_n \cos \theta + k_{2y'} \sin \alpha$  and  $\Delta k_y \equiv -2k_{1y} - G_n \sin \theta + k_{2y'} \cos \alpha$ , which are related to the linear momenta and the reciprocal vectors provided by the spatially modulated crystals. For SHG of vortex beams, the two parameters are approximately constant when the transverse wave vectors are small. When the interacting waves are both perpendicular to the ferroelectric domain walls [i.e.,  $\theta = 90^\circ$  and  $\alpha = 0^\circ$  in Fig. 1(a)], this gives the well-known collinear quasi-phase-matched SHG [18]. Nonlinear Bragg diffraction [19] occurs when the longitudinal and transverse phase-matching conditions are both fulfilled, i.e.,  $\Delta k_x = \Delta k_y = 0$ . Nonlinear Raman-Nath diffraction [20,26,27] corresponds to another special type of noncollinear phase-matching diagram in which the transverse component is

phase matched ( $\Delta k_x = 0$ ), while the longitudinal direction is phase mismatched ( $\Delta k_y \neq 0$ ). In the experiment, one can rotate the nonlinear crystal around the  $z$  axis to switch the phase-matching diagrams. In addition, the phase mismatch can be tuned by changing the working temperature, as well as choosing the diffraction orders. Thus, periodically poled crystals provide a flexible platform to investigate the characteristics as well as to gain insight into the underlying physics for frequency conversion of such light beams.

The nonlinear wave equation governing the SHG process can be solved using the Green-function formalism [28], and the generated SH at  $2\omega$  in the far field can be regarded as the Fourier transform of the FW from real space to reciprocal space. If we assume that the FW is in the form of an  $l$ th-order LG mode with radial index zero, and make the small-angle approximation  $\sin^2 \alpha \approx 0$  ( $\alpha < 15^\circ$ ), then the SH field for the several aforementioned phase-matching diagrams can be written as the following unified form (see Supplemental Material, Sec. I for details [29]):

$$E^{(2\omega)} \propto L \operatorname{sinc}[(\Delta k_y L - L k_{2r'} \sin \alpha \cos \phi')/2] u(k_{2r'}) e^{i2l\phi'}, \quad (2)$$

with

$$u(k_{2r'}) = (w_0 k_{2r'})^{2|l|} {}_1F_1[1 + 2|l|; 1 + 2|l|; -(w_0 k_{2r'})^2/8] \quad (3)$$

in which  ${}_1F_1(a; b; z)$  is the confluent hypergeometric function [31].  $w_0$  is the beam waist of the FW.  $L = L_1/\cos \theta$  is the interaction length of the noncollinear SHG process in the nonlinear crystal, while  $L = L_2$  for the collinear case. From Eq. (2) we can see that the electric field of the SH wave is determined by the phase-matching condition defined by both the linear momentum and OAM. The intensity distribution of the SH wave has a ring-shaped envelope  $u(k_{2r'})$  and is modulated by the sinc function. There is a spiral phase term  $e^{i2l\phi'}$  in the electric field distribution of the SH wave, where the index is twice that of the FW. Moreover, the azimuth-dependent phase mismatch in the sinc function will affect the angular phase and intensity distribution of the SH wave, and by decomposing the sinc function in terms of spiral harmonics  $e^{-im\phi'}$  (where  $m$  is an integer), OAM sidebands around the center number  $2l$  will be generated on the SH wave.

For collinear SHG, where  $\theta = \pi/2$  and  $\alpha = 0$ , the profile of the SH wave can be expressed as

$$E^{(2\omega)}(k_{2r'}, \phi') \propto L_2 \operatorname{sinc}[(2k_{1y} + G_n - k_{2y'})L_2/2] \times u(k_{2r'}) e^{i2l\phi'} \quad (4)$$

In Eq. (4), the phase-mismatch term in the sinc function is independent of the azimuthal angle  $\phi'$ , and the only term

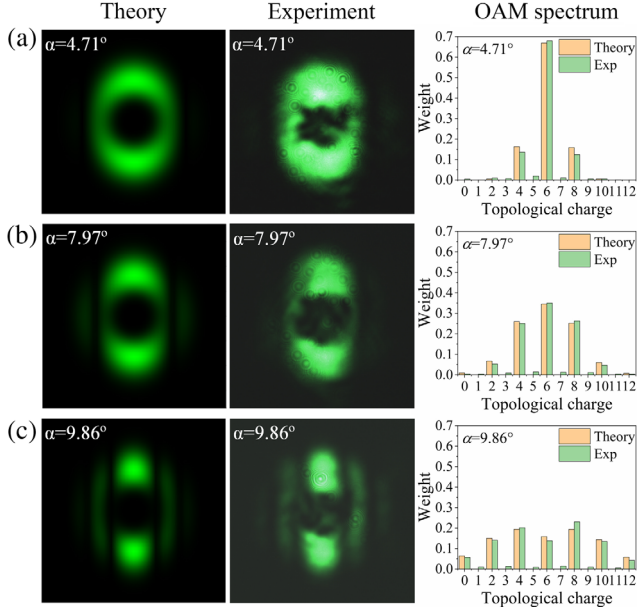


FIG. 2. Intensity profiles and OAM spectra of SH waves from (a) third-, (b) fifth-, and (c) sixth-order nonlinear Bragg diffraction with the TC of the FW being  $l = 3$ . The corresponding diffraction angles are  $4.71^\circ$ ,  $7.97^\circ$ , and  $9.86^\circ$  respectively.

containing  $\phi'$  is the spiral phase term  $e^{i2l\phi'}$ . Choosing an OAM basis  $\langle m |$ , we can evaluate the probability amplitude of each OAM component:

$$\begin{aligned}
 a(m) &= \langle m | E^{(2\omega)} \rangle \\
 &\propto L_2 \text{sinc}[(2k_{1y} + G_n - k_{2y'})L_2/2] 2\pi \delta_{m,2l} \\
 &\quad \times \int_0^{+\infty} u(k_{2r'}) k_{2r'} dk_{2r'}. \quad (5)
 \end{aligned}$$

In Eq. (5), the inner product is nonzero only when  $m = 2l$ , which indicates that the SH wave has a single OAM value which is twice that of the FW. In addition, the longitudinal wave vector mismatch only influences the SHG efficiency, and it does not affect the OAM distribution in collinear SHGs. Our experimental results on quasi-phase-matched and mismatched collinear SHG of vortex beams are consistent with previous reports. See Supplemental Material, Secs. 2 and 3 for details [29].

An experiment on SHG of vortex beams in a Bragg diffraction configuration was carried out in a periodically poled KTP (PPKTP) with a poling period of  $10.125 \mu\text{m}$  (see Supplemental Material, Sec. IV for details [29]), and several orders of nonlinear Bragg diffractions could be obtained by rotating the crystal around the  $z$  axis. The recorded profiles of the SH waves are shown in Fig. 2. We can see that the intensity profiles of the SH waves from the nonlinear Bragg diffraction have an intensity null in the beam center, just as predicted. Because  $\Delta k_y = 0$ , vertical dark stripes appear at the zeros of the modulating function  $\text{sinc}(-Lk_{2r'} \sin \alpha \cos \phi'/2)$  in Eq. (2), where the

destructive interference of the SH occurs when the phase difference accumulated by the longitudinal phase mismatch reaches a nonzero integer multiple of  $\pi$ . As the noncollinear angle  $\alpha$  increases, the maximum value of the phase term in the sinc function will increase correspondingly, and thus the first-order dark stripe will move toward the center of the SH spot and more dark stripes will appear. We studied the third-, fifth-, and the sixth-order nonlinear Bragg diffractions when the TC of the FW was  $l = 3$ ; the corresponding diffraction angles were  $4.71^\circ$ ,  $7.97^\circ$ , and  $9.86^\circ$ , respectively. The first and second columns in Fig. 2 give the theoretical and measured intensity profiles of the SH waves with different diffraction angles, which were consistent with the above analysis.

The weight of each OAM components of the SH wave from nonlinear Bragg diffraction can be written as

$$\begin{aligned}
 a(m) &\propto \int_0^{+\infty} \int_0^{2\pi} \text{sinc}(c \cos \phi') e^{i(2l-m)\phi'} d\phi' u(k_{2r'}) \\
 &\quad \times k_{2r'} dk_{2r'}, \quad (6)
 \end{aligned}$$

in which  $c = -Lk_{2r'} \sin \alpha/2$ . According to the Taylor series of the sinc function,  $\text{sinc}(c \cos \phi') = \sum_{j=0}^{+\infty} (-1)^j \times (c \cos \phi')^{2j+1} / (2j+1)!$ , we can obtain a nontrivial solution only if  $m-2l$  is even. This means that only even-order spiral harmonics will contribute to the OAM spectrum, as can be seen clearly from the OAM spectra of the SH waves in the last column of Fig. 2. In nonlinear Bragg diffraction, the SH field distributions still have a high degree of symmetry, being symmetrical about the vertical and horizontal axes. The OAM distribution, concentrating on the even-order components while missing the odd-order components, reflects the symmetry of the SH fields. With increasing diffraction angle  $\alpha$ , the weights of the high-order terms in the series expansion become larger, and thus the probability of the central OAM component decreases while the probabilities of the neighboring even-order components increase.

When the temperature of the nonlinear crystal was tuned off the phase-matching temperature point, the parameter  $\Delta k_x$  remained zero, while  $\Delta k_y$  became nonzero. In this case, the phase-matching diagram can be looked upon as the nonlinear Raman-Nath diffraction. In the experiment, the temperature of the nonlinear crystal was changed from  $70^\circ\text{C}$  to  $110^\circ\text{C}$  in steps of  $10^\circ\text{C}$ , and the values of  $\Delta k_y$  at each temperature point are listed in Table I. The intensity

TABLE I. Phase-mismatch term  $\Delta k_y$  at different temperatures for Raman-Nath diffractions.

	Temperature of nonlinear crystal ( $^\circ\text{C}$ )				
	70.0	80.0	90.0	100.0	110.0
$\Delta k_y$ ( $\mu\text{m}^{-1}$ )	-0.0028	-0.0014	0.0	0.0015	0.0030

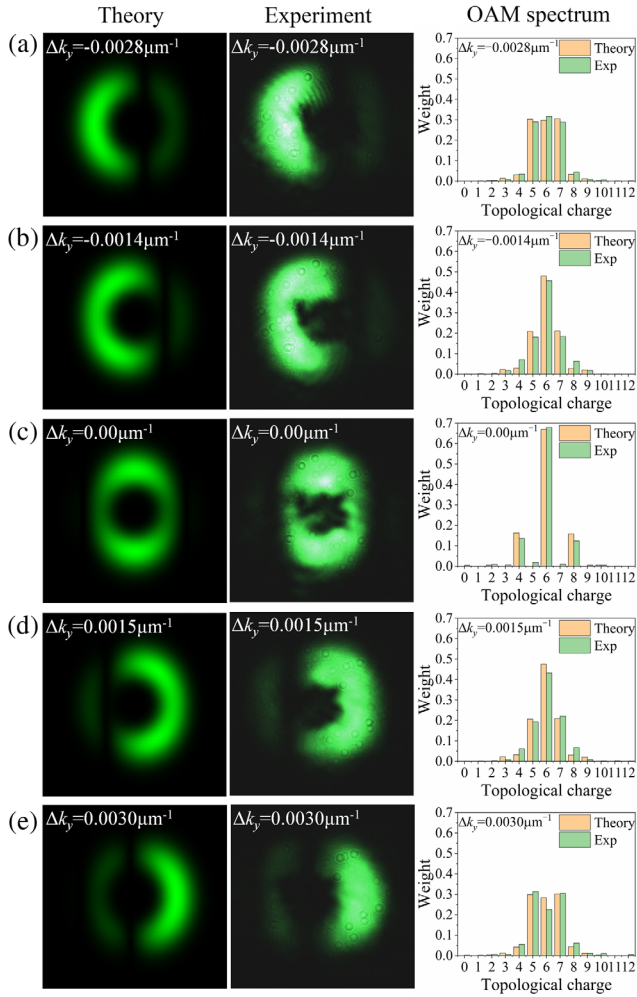


FIG. 3. Intensity profiles and OAM spectra of SH waves with different phase mismatch  $\Delta k_y$ . For comparison, nonlinear Bragg diffraction with  $\Delta k_y = 0.0$  is shown in (c), and cases of nonlinear Raman-Nath diffraction are shown in (a), (b), (d), and (e). The TC of the FW is  $l = 3$ .

profiles together with the OAM spectra from the third-order Raman-Nath diffraction are shown in Fig. 3. In contrast to the case of nonlinear Bragg diffraction, the field distribution of the SH wave from Raman-Nath diffraction is not symmetric about the vertical axis. With a different sign of the phase mismatch  $\Delta k_y$ , the dark stripe appeared on a different side of the beam center. Moreover, the dark stripe moved toward the spot center with increasing  $\Delta k_y$ . Owing to the nonzero  $\Delta k_y$ , which is independent of the azimuthal angle  $\phi'$ , the series expansion of the function  $\text{sinc}[(\Delta k_y L - L k_{2\phi'} \sin \alpha \cos \phi')/2]$  contains both even and odd terms, which can be seen from the calculated and measured OAM spectra in Fig. 3.

To obtain more pronounced Raman-Nath diffraction of vortex beams, we used another piece of PPKTP crystal with a poling period of  $2.55 \mu\text{m}$  to introduce larger phase mismatches  $\Delta k_y$ . The FW with a TC of 1 was incident

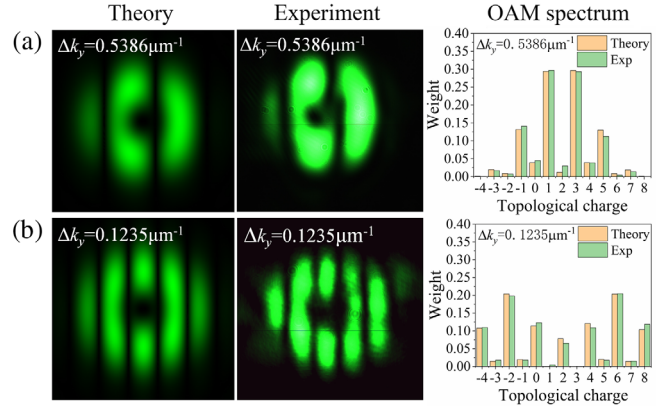


FIG. 4. Intensity profiles and OAM spectra of SH waves for (a) first- and (b) second-order Raman-Nath diffraction from a short-pitched PPKTP; the corresponding phase mismatches  $\Delta k_y$  are shown in each panel. The TC of the FW is  $l = 1$ .

on the nonlinear crystal along the direction parallel to the ferroelectric domain wall, and the first- and second-order SH Raman-Nath diffractions could be observed, the corresponding diffraction angles being  $6.14^\circ$  and  $12.69^\circ$ , respectively. Because of the large diffraction angles, as well as the large phase mismatches ( $0.5386$  and  $0.1235 \mu\text{m}^{-1}$ ), multiple dark stripes appeared in the SH intensity profiles, as shown in Fig. 4. Moreover, odd- and even-order components dominated, respectively, with different diffraction orders, which differed from the situation with small phase mismatches. This can be qualitatively analyzed as follows. Because  $\Delta k_y \gg k_{2\phi'} \sin \alpha \cos \phi'$ , the sinc function is approximately equal to  $2 \sin(\Delta k_y L/2 + c \cos \phi')/(\Delta k_y L)$ , which can be simplified to  $2 \sin(c \cos \phi')/(\Delta k_y L)$  or  $2 \cos(c \cos \phi')/(\Delta k_y L)$  when the phase accumulated by  $\Delta k_y L/2$  approaches even or odd multiples of  $\pi/2$ . Thus, the OAM components are determined by the coefficients in the series expansion of the sine or cosine function, respectively. See Supplemental Material, Sec. V for a detailed analysis [29].

In conclusion, we have demonstrated that OAM transfer in frequency conversions is dictated by the phase-matching condition defined by both the linear and orbital angular momenta. Several phase-matching diagrams, such as collinear SHG, nonlinear Bragg diffraction, and nonlinear Raman-Nath diffraction have been exploited in periodically poled crystals to tune the phase-matching condition imposed on SHG of vortex beams. The OAM spectrum is determined by the longitudinal phase mismatch, or more specifically by the spiral harmonics provided by the phase-mismatch term. If the longitudinal phase mismatch is totally independent of the azimuthal angle, then the SH wave will carry a single OAM which is twice that of the FW. There exist only even-order OAM components when the longitudinal phase mismatch contains a single term that

is dependent of the azimuthal angle. An OAM spectrum with index covering the full integer range is obtained when both the azimuth-dependent and azimuth-independent terms are included. The results presented here can help in understanding the OAM transfer mechanism in nonlinear frequency conversions. Moreover, our work can open an avenue to flexible tailoring of the OAM spectrum at desired wavelengths, which has important potential applications such as OAM mode multicasting in optical communications and high-dimensional spatial mode entanglement in quantum information technology.

Small-angle approximation was used to give explicit expressions of the OAM spectrum, however, the theoretical treatment developed in this paper is also applicable for the situations with large noncollinear angles, as well as for investigation of frequency conversion of structured lights. In this work, we experimentally demonstrate the phase-matching controlled nonlinear OAM conversion in periodically poled crystals. The physical mechanism can be further applied to other nonlinear platforms such as nonlinear metasurface [34]. Interestingly, lithium niobate thin film emerges recently as a promising platform to utilize the advantages of both metasurface and periodically poled crystal, which may provide flexible phase matching configuration for nonlinear manipulation of OAM states.

The work was supported financially by the National Key R&D Program of China (No. 2019YFA0705000 and No. 2017YFA0303700), National Natural Science of China (No. 11674171, No. 91950206, No. 11627810, and No. 51890861), the Leading-edge Technology Program of Jiangsu Natural Science Foundation (No. BK20192001), the Key R&D Program of Guangdong Province (No. 2018B030329001), and the Fundamental Research Funds for the Central Universities (No. 021314380177). The authors also thank Professor Minghui Lu, from Nanjing University, for support in providing the picosecond laser.

\*These authors contributed equally to this work.

<sup>†</sup>xphu@nju.edu.cn

<sup>\*</sup>zhangyong@nju.edu.cn

<sup>§</sup>zhusn@nju.edu.cn

- [1] J. A. Armstrong, N. Bloembergen, J. Ducuing, and P. S. Pershan, *Phys. Rev.* **127**, 1918 (1962).
- [2] N. Bloembergen, *J. Opt. Soc. Am.* **70**, 1429 (1980).
- [3] L. Allen, M. W. Beijersbergen, R. J. C. Spreeuw, and J. P. Woerdman, *Phys. Rev. A* **45**, 8185 (1992).
- [4] A. Yao and M. J. Padgett, *Adv. Opt. Photonics* **3**, 161 (2011).
- [5] Y. J. Shen, X. J. Wang, Z. W. Xie, C. J. Min, X. Fu, Q. Liu, M. L. Gong, and X. C. Yuan, *Light Sci. Appl.* **8**, 90 (2019).
- [6] M. Erhard, R. Fickler, M. Krenn, and A. Zeilinger, *Light Sci. Appl.* **7**, 17146 (2018).
- [7] N. V. Bloch, K. Shemer, A. Shapira, R. Shiloh, I. Juwiler, and A. Arie, *Phys. Rev. Lett.* **108**, 233902 (2012).
- [8] G. Garipey, J. Leach, K. T. Kim, T. J. Hammond, E. Frumker, R. W. Boyd, and P. B. Corkum, *Phys. Rev. Lett.* **113**, 153901 (2014).
- [9] L. Rego, J. S. Román, A. Picón, L. Plaja, and C. Hernández-García, *Phys. Rev. Lett.* **117**, 163202 (2016).
- [10] A. Aadhi, G. K. Samanta, S. C. Kumar, and M. Ebrahim-Zadeh, *Optica* **4**, 349 (2017).
- [11] Z. Y. Zhou, S. L. Liu, Y. Li, D. S. Ding, W. Zhang, S. Shi, M. X. Dong, B. S. Shi, and G. C. Guo, *Phys. Rev. Lett.* **117**, 103601 (2016).
- [12] X. D. Qiu, F. S. Li, W. H. Zhang, Z. H. Zhu, and L. X. Chen, *Optica* **5**, 208 (2018).
- [13] B. Sephton, A. Vallés, F. Steinlechner, T. Konrad, J. P. Torres, F. S. Roux, and A. Forbes, *Opt. Lett.* **44**, 586 (2019).
- [14] S. Li, L. J. Kong, Z. C. Ren, Y. Li, C. Tu, and H. T. Wang, *Phys. Rev. A* **88**, 035801 (2013).
- [15] W. T. Buono, A. Santos, M. R. Maia, L. J. Pereira, D. S. Tasca, K. Dechoum, T. Ruchon, and A. Z. Khoury, *Phys. Rev. A* **101**, 043821 (2020).
- [16] K. Dholakia, N. B. Simpson, M. J. Padgett, and L. Allen, *Phys. Rev. A* **54**, R3742 (1996).
- [17] J. Courtial, K. Dholakia, L. Allen, and M. J. Padgett, *Phys. Rev. A* **56**, 4193 (1997).
- [18] S. M. Saitiel, A. A. Sukhorukov, and Y. S. Kivshar, *Prog. Opt.* **47**, 1 (2005).
- [19] S. M. Saitiel, D. N. Neshev, R. Fischer, W. Krolikowski, A. Arie, and Y. S. Kivshar, *Phys. Rev. Lett.* **100**, 103902 (2008).
- [20] S. M. Saitiel, D. N. Neshev, W. Krolikowski, A. Arie, O. Bang, and Y. S. Kivshar, *Opt. Lett.* **34**, 848 (2009).
- [21] X. P. Hu, P. Xu, and S. N. Zhu, *Photonics Res.* **1**, 171 (2013).
- [22] A. Shapira, I. Juwiler, and A. Arie, *Laser Photonics Rev.* **7**, L25 (2013).
- [23] X. P. Hu, Y. Zhang, and S. N. Zhu, *Adv. Mater.* **31**, 1903775 (2019).
- [24] D. Z. Wei, C. Wang, X. Xu, H. Wang, Y. Hu, P. Chen, J. Li, Y. Zhu, C. Xin, X. P. Hu, Y. Zhang, D. Wu, J. Chu, S. N. Zhu, and M. Xiao, *Nat. Commun.* **10**, 4193 (2019).
- [25] S. Liu, K. Switkowski, C. L. Xu, J. Tian, B. X. Wang, P. X. Lu, W. Krolikowski, and Y. Sheng, *Nat. Commun.* **10**, 3208 (2019).
- [26] S. M. Saitiel, D. N. Neshev, W. Krolikowski, N. Voloch-Bloch, A. Arie, O. Bang, and Y. S. Kivshar, *Phys. Rev. Lett.* **104**, 083902 (2010).
- [27] Y. Sheng, W. Wang, R. Shiloh, V. Roppo, A. Arie, and W. Krolikowski, *Opt. Lett.* **36**, 3266 (2011).
- [28] C. Yao, F. J. Rodriguez, J. Bravo-Abad, and J. Martorell, *Phys. Rev. A* **87**, 063804 (2013).
- [29] See Supplemental Material at <http://link.aps.org/supplemental/10.1103/PhysRevLett.125.143901> for (i) the derivation of Eq. (2) in the main text, (ii) the experimental results for collinear SHG of vortex beams, (iii) the method for measuring the OAM spectrum, (iv) the experimental setup for noncollinear SHG of vortex beams, and (v) the analysis of the OAM spectrum of the SH waves from nonlinear Raman-Nath diffraction with large phase mismatch, which includes Refs. [28,30–33].

- [30] G. N. Watson, *A Treatise on the Theory of Bessel Functions* (Cambridge University Press, Cambridge, England, 1996).
- [31] H. Buchholz, The Confluent Hypergeometric Function, in *Springer Tracts in Natural Philosophy* Vol. 15 (Springer-Verlag, Berlin, 1969).
- [32] R. Ni, Y. F. Niu, L. Du, X. P. Hu, Y. Zhang, and S. N. Zhu, *Appl. Phys. Lett.* **109**, 151103 (2016).
- [33] J. Řeháček, Z. Bouchal, R. Čelechovský, Z. Hradil, and L. L. Sánchez-Soto, *Phys. Rev. A* **77**, 032110 (2008).
- [34] T. Pertsch and Y. Kivshar, *MRS Bull.* **45**, 210 (2020).